and a perturbation

$$H_1=\lambda\left\{\frac{1}{2}\int\psi^\dagger(\mathbf{x})\psi^\dagger(\mathbf{x}')v(\mathbf{x},\mathbf{x}')\psi(\mathbf{x}')\psi(\mathbf{x})d\mathbf{x}d\mathbf{x}'-\int\psi^\dagger(\mathbf{x})V_{\text{eff}}(\mathbf{x},\mathbf{x}')\psi(x')d\mathbf{x}d\mathbf{x}'+\tfrac{1}{2}\sum_{nm}{}'Z_nZ_mv(\mathbf{R}_n,\mathbf{R}_m)\right\}. \quad \text{(B16)}$$

V_{eff} can be chosen quite arbitrary but we may think of a Hartree potential plus Coulomb-hole and screened-exchange potentials. The $\Delta E(G)$ corresponding to H_1 of Eq. (16) is given by Eq. (B14) plus two additional terms,

$$\Delta E(G)=\text{Eq. (B14)}+i\int\frac{d\epsilon}{2\pi}e^{i\epsilon\Delta}\,\text{Tr}(V_{\text{eff}}G(\epsilon))+\tfrac{1}{2}\sum_{nm}{}'Z_nZ_mv(\mathbf{R}_n,\mathbf{R}_m). \quad \text{(B17)}$$

The G_0 of Eq. (B14) now of course corresponds to Eq. (B15). It is easily checked that Eq. (B17) gives the correct energy shift and equation for G.

The unperturbed energy corresponding to Eq. (B15) is simply the sum of the N smallest eigenvalues of the one-electron operator $h+V_{\text{eff}}$. While this generally is not a good approximation of the true energy, it is on the other hand not very far off. *The importance of the split into H_0+H_1 lies however in the fact that G_0 has now become quite realistic.* Specifically, if we approximate G by G_0 in Eq. (B17) we find that the V_{eff} G term cancels against the same term in E_0 and that the last integral in Eq. (B14) vanishes. The GGv term is the Coulomb energy and the $\ln(1-Pv)$ term gives in the lowest approximation the HF exchange energy. If we want, we can gradually improve V_{eff} to make G_0 more closely like G. This is, however, only possible up to a certain point since V_{eff} is energy-independent.

PHYSICAL REVIEW VOLUME 139, NUMBER 3A 2 AUGUST 1965

Cyclotron Resonance in Cadmium

J. K. Galt, F. R. Merritt, and J. R. Klauder
Bell Telephone Laboratories, Murray Hill, New Jersey

(Received 8 March 1965)

Extensive observations at 1.5°K and both 23.8 Gc/sec and 74.2 Gc/sec of cyclotron-resonance phenomena in cadmium are reported. One group of experiments is done with the steady applied field parallel to the sample plane (Azbel'-Kaner geometry). A large number of signals are observed, only some of which are sufficiently reliable to identify with cyclotron masses. All the masses are plotted versus the crystallographic orientation of the steady applied field in three of the principal planes. The reliable, well resolved signals are identified and associated tentatively with orbits. Most of these orbits are consistent with the current model of the Fermi surface of cadmium, but some of them require small modifications of it. These orbits are either on the "pillow" or on the large surface associated with holes in the second band. The masses observed with the magnetic field parallel to the sample plane are all too large to identify plausibly with the smaller pieces of the Fermi surface such as the "butterflies" and "cigars". It is suggested that the resonances associated with the charge carriers of smaller mass are lost in the signals from harmonics of those of larger mass. In another group of experiments, data have been obtained with the steady applied field normal to the sample surface. Here signals are obtained at classical cyclotron-resonance fields equal to those observed in the other geometry although the signals are in the anomalous-skin-effect regime and the much larger effects associated with Doppler-shifted cyclotron resonance are at magnetic fields too high to be observed. A theoretical treatment and a discussion of the physics of these effects is given. In this geometry, a cyclotron mass of approximately 0.22 m_0 is also observed. The related orbit is only tentatively identified, but it is definitely thought to involve one of the smaller pieces of the Fermi surface.

I. INTRODUCTION

EXTENSIVE observations of cyclotron resonance in cadmium obtained by plotting the variation of surface absorption coefficient as a function of steady applied magnetic field are presented in this paper and interpreted in terms of current theoretical understanding of the Fermi surface. The experimental results given here extend previously reported preliminary studies on this metal.[1] Data were obtained at 1.5°K at frequencies near both 23.8 Gc/sec and 74.2 Gc/sec. Most of the data were obtained at various crystallographic orientations with the steady applied magnetic field parallel to the plane sample surface, i.e., in the Azbel'-Kaner geometry.[2] From these data, plots of cyclotron masses as a function of crystallographic orientation were made. In addition, data have been obtained for selected crystallographic orientations with the steady applied field normal to the plane sample

[1] J. K. Galt, F. R. Merritt, and P. H. Schmidt, Phys. Rev. Letters **6**, 458 (1961).

[2] M. Ya Azbel' and E. A. Kaner, Zh. Eksperim. i Teor. Fiz. **30**, 811 (1956) [English transl.: Soviet Phys.—JETP **3**, 772 (1956)]; J. Phys. Chem. Solids **6**, 113 (1958).

surface. These results determine for at least some of the charge carriers whether they are holes or electrons. They also throw light on wave propagation in the plasma formed by the Fermi sea.

Theoretical studies[3,4] have provided a model for the band structure of the hexagonal close-packed metals and there is already some experimental data on de Haas–van Alphen effect and magnetoacoustic attenuation in cadmium relevant to this model in the literature.[5–9] The interpretation of these earlier data has given a considerable amount of information on the Fermi surface of cadmium. The cyclotron resonance results give primarily information on the effective mass of the various charge carriers as a function of crystallographic direction, and from this on the anisotropy of the Fermi surface. Information on the latter point is gained from the relation[10,11]

$$m^* = (\hbar^2/2\pi)(\partial S/\partial E), \tag{1}$$

where m^* is the cyclotron mass, S is the cross-sectional area normal to the applied steady magnetic field of the relevant section of Fermi surface in k space, and E is the energy of the charge carrier.

The Fermi surface in cadmium is made up of many pieces, one of which has a very complicated re-entrant shape. As a result, there are many different signals present in the data for a single crystallographic orientation, each a result of a distinct set of orbits. The large number of these signals is especially apparent from the data obtained with the steady applied field parallel to the sample surface. In these data, some of the signals are well resolved and unambiguous, but some are not. Consequently, the reliability of the interpretation of the signals varies greatly from one of them to another. The data are presented in Sec. III so as to emphasize the signals which are large and well resolved. These data are discussed in Sec. IV and interpreted as far as possible in terms of the present theoretical model of the Fermi surface in cadmium mentioned above. In this section also, the more reliable signals are emphasized.

The data obtained with the magnetic field normal to the sample surface are also presented in Sec. III. In this case fewer signals are resolved than in the other geometry. These signals occur at the classical cyclotron-resonance field, in spite of the fact that the experiments are done in the anomalous-skin-effect regime. This fact is at first puzzling in terms of current theories of the surface impedance of metals in the anomalous skin effect regime. It is shown in Sec. IV, however, that the relatively small signals observed can be explained by higher order terms in these theories.

II. EXPERIMENTAL

The microwave technique used in these experiments is very similar to one previously reported,[12] and it will, therefore, be described only briefly. The crystallographically oriented plane surface of a disk sample is made to form part of the end wall of a cylindrical cavity operating in the TE_{112} (at 23.8 Gc/sec) or TE_{113} (74.2 Gc/sec) mode. The E field in these modes is everywhere normal to the cylindrical axis of the cavity, and the mode frequencies are degenerate with respect to the rotational position of this E-field pattern about the cylindrical axis. As a result, it is possible to couple the cavity at a point on the broad side of a standard waveguide such that the E field is circularly polarized on the cavity axis. This has been done in most of the experiments reported here. In order to achieve adequate sensitivity, the sample extends a significant distance from the center out along the radius of the cavity end wall, with the result that the polarization of the radiation is not perfectly circular. Observations of paramagnetic resonance in a small calcium copper acetate sample placed at various points on the cavity-end wall showed that the power density of the undesired circular polarization averaged over the sample is 10% or less of the desired one in the experiments reported here. The cavity can also be coupled to the broad side of the waveguide at such a point that the radiation incident on the sample is linearly polarized. This has been done in certain experiments, the results of which are mentioned briefly. In general, however, circularly polarized radiation is used, and this should be assumed unless explicit reference to polarization is made. The variations in the signal which passes the cavity are observed as a function of the steady applied magnetic field, B_0. The experimentally observed quantity, in this cavity arrangement, is proportional to the variation in the power-absorption coefficient of the sample surface.

There are, however, some differences between the present microwave experimental arrangements and those reported earlier.[12] First, the cavity is enclosed in a can which excludes the liquid helium from it. This reduces the noise level in the system and thereby improves the effective sensitivity. Second, the cavity position is different for most, but not all of the experiments reported here. Although still mounted on the broad side of the waveguide, it is at the bottom of the U into which the waveguide is bent. As a result, its end walls are horizontal rather than vertical, and the sample,

[3] W. A. Harrison, Phys. Rev. **118**, 1190 (1960); **126**, 497 (1962).
[4] L. M. Falicov and M. H. Cohen, Phys. Rev. **130**, 92 (1963).
[5] T. G. Berlincourt, Phys. Rev. **94**, 1172 (1954).
[6] A. S. Joseph, W. L. Gordon, J. R. Rietz, and T. G. Eck, Phys. Rev. Letters **7**, 334 (1961).
[7] J. D. Gavenda and B. C. Deaton, Phys. Rev. Letters **8**, 208 (1962).
[8] L. Mackinnon, M. T. Taylor, and M. R. Daniel, Phil. Mag. **7**, 523 (1962); L. Mackinnon and M. R. Daniel, Phys. Letters **1**, 157 (1962).
[9] D. F. Gibbons and L. M. Falicov, Phil. Mag. **8**, 177 (1963).
[10] W. Shockley, Phys. Rev. **90**, 491 (1953).
[11] I. M. Lifshits and A. M. Kosievitch, Zh. Eksperim. i Teor. Fiz. **29**, 730 (1955) [English transl.: Soviet Phys.—JETP **2**, 636 (1956)].
[12] J. K. Galt, W. A. Yager, F. R. Merritt, B. B. Cetlin, and A. D. Brailsford, Phys. Rev. **114**, 1396 (1959).

which forms part of one of these end walls, is in a horizontal plane. In this position, with circularly polarized radiation incident upon the sample, data with B_0 in the plane of the sample can be obtained as a function of the crystallographic orientation of B_0 in this plane by simply rotating the magnet about a vertical axis. This method was used to obtain the plots of cyclotron mass versus crystallographic orientation presented in Sec. III.

The position of the cavity was adjusted carefully in these experiments to assure that the plane of the sample was always horizontal to within $\pm 0.1°$. The plane of rotation of the magnet was horizontal to within $\pm 0.25°$. Thus the magnetic field was within $\pm 0.35°$ of the plane of the sample in all cases. An exploration of the way the magnet tilt varied with rotational position showed that the average value was $\pm 0.1°$ so that the average total error was about $\pm 0.15°$. These adjustments were made to minimize such effects as the splitting of peaks in the data observed in various cyclotron resonance experiments on potassium, aluminum, copper and tin.[14] Further comments on the relation of this phenomenon to our data are made below.

A vital part of the success in observing cyclotron resonance in cadmium is the preparation of suitable samples. We therefore describe the essential steps in this process. The starting material was "High Purity" grade cadmium obtained from United Mineral and Chemical Corporation in $\frac{1}{2}$-in.-diameter rods, $8\frac{1}{2}$ in. long. Each such rod was given 10 to 12 zone refining passes in a carefully cleaned silica boat which was coated with carbon on those surfaces which made contact with the cadmium. This material was then melted under vacuum in a carefully cleaned environment in such a geometry that it then flowed through a vycor funnel into a carefully cleaned and vacuum fired graphite crucible where it again solidified. The cylindrical space inside this crucible was formed to produce a point at the bottom, and the cadmium was thus formed into a boule pointed at one end. The crucible with the boule in it was sealed off under vacuum inside a silica tube. This assembly was then lowered through a furnace at about 1.6 in. per h. The crystals produced in this way show residual resistance ratios $R_{273°K}/R_{4.2°K}$ of 27 000 to 40 000. These crystals were crystallographically oriented by x-ray techniques, and oriented disk samples cut from them with an acid string saw. The surfaces of the disks were finally smoothed by light rubbing on a cotton cloth impregnated with nitric acid. In this last process, it is important to limit the temperature rise of the sample caused by the acid-cadmium reaction in order to produce a flat rather than a convex surface. This is accomplished by frequent water rinses, and by supporting the work on a metal rather than a glass base so that heat is rapidly conducted away from the point of contact. Tests on the final disks with straight edges have shown them to be flat to approximately one minute of arc. Their short-range roughness was such that it cannot be determined by producing Newton's rings, but observations with a high-powered microscope indicate that they were smooth to approximately 10^{-4} cm. X-ray observations with a double crystal spectrometer on an individual Laue reflection from these samples have shown that there is substantially no mosaic structure or strain in these samples. Such distortions do occur when crystals of cadmium are produced by the Czochralski technique.

III. RESULTS

Data with the magnetic field parallel to the sample plane were taken every 2.5° as the steady applied field was rotated in each of three crystallographic planes through an angular interval which included all nonequivalent directions in each plane. These angular intervals are from $\langle 0001 \rangle$ to $\langle 11\bar{2}0 \rangle$ in the $(10\bar{1}0)$ plane, from $\langle 0001 \rangle$ to $\langle 10\bar{1}0 \rangle$ in the $(11\bar{2}0)$ plane, and from $\langle 11\bar{2}0 \rangle$ to $\langle 10\bar{1}0 \rangle$ in the (0001) plane. Observation of both the variation of the surface absorption coefficient with the magnitude of B_0 and of the derivative of this quantity was made in each case at both 23.8 and 74.2 Gc/sec. At all observed orientations, many signals are present, each of the largest of which determines an effective mass easily and unamibguously. However, the weakness of a signal in many cases makes its identification from a single observation uncertain. A signal which identifies one effective mass and is observed in all four of the experiments done at one crystallographic orientation (direct observation and derivative method at each of two frequencies) is regarded as satisfactorily determined. This is by no means always possible. In general, the derivative observations give better resolution; therefore, a signal at one orientation observed unequivocally at both frequencies with the derivative method is considered reliable. Unfortunately, the data indicate that many signals are present which are not well enough resolved for this to be true either, and unambiguous identification of the relevant effective mass is not possible. In such situations, it has been useful to examine and compare the data for neighboring crystallographic orientations. In this way, it has been possible to make a tentative identification of many masses for which the evidence obtained at any one angle is inadequate.

These remarks are illustrated by the data in Figs. 1 and 2, which show the experimental data obtained at both frequencies when B_0 is in the $(11\bar{2}0)$ plane at an angle of 58° with the hexagonal axis. All the field values for which the data give evidence of a resonance are identified by arrows at the bottom of the figures. The top curve in each case is a derivative curve in which the resonances are identified with peaks. On the lower curves, resonances are associated with points of maximum slope. In Fig. 2, some resonances are outside the available field range, so the arrows identify second harmonics rather than fundamental resonances, as indi-

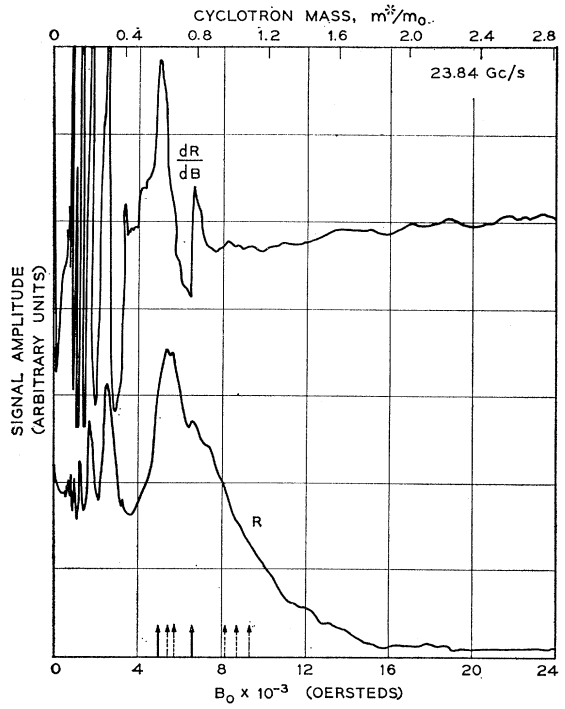

FIG. 1. Example of raw data obtained at 23.8 kMc/sec and 1.5°K. These data were obtained with the steady applied magnetic field B_0 at the crystallographic orientation represented by 58° in Fig. 4, as were those shown in Fig. 2. The lower curve shows the variation in the surface impedance R of cadmium on an arbitrary scale as a function of B_0 under these conditions directly on an arbitrary scale. The upper curve shows an experimentally observed derivative of this same quantity with respect to magnetic field, dR/dB, also on an arbitrary scale. The variation observed very near zero field has not been studied in detail, but is thought to be due to sample heating. The cyclotron mass corresponding to resonance at each value of B_0 is plotted at the top of the figure.

cated. The two solid arrows identify two resonances for which the evidence is quite unambiguous. For both of these resonances, several harmonics are observed and a plot of the number of the harmonic versus $1/B_0$ is linear to well within the experimental uncertainty in B_0. These two resonances are observed in all four runs in Figs. 1 and 2, and the mass values derived independently from the data at the two different frequencies are identical. The dashed arrows identify signals which are not so reliable. The evidence for them in Figs. 1 and 2 varies, but data at neighboring orientations confirm the indications given here. Note that all the masses identified in Fig. 1 are also identified in Fig. 2. The higher frequency at which the data shown in Fig. 2 were obtained makes possible the tentative identification of two more signals than in Fig. 1, one of them indicated by two arrows bound together by a dashed line to indicate uncertainty about the resonance field. The evidence for these weaker signals includes indications of harmonics which are not easy to identify in Figs. 1 and 2, but which can be seen better, although with varying degrees of reliability, in the original data.

The number of signals present, and the uncertainties associated with them, have made it impossible to analyze the raw data for cyclotron masses by fitting the experimental curves to theoretical ones. Instead, we have identified masses from the values of B_0 at the peaks in the derivative curves, as indicated in Figs. 1 and 2. In connection with the theory of such curves, however, it should be mentioned that the shape of those obtained in these experiments differs noticeably from that expected from the Azbel'-Kaner theory of cyclotron resonance in this geometry in that the peaks in the variation of surface impedance are more rounded. We have no satisfactory explanation of this fact. We note that the observed shape bears a noticeable similarity to that derived by Jones and Sondheimer[13] and one possibility is that their calculation is relevant. The conditions of our experiments do not fit their assumptions well, however. Partly for later reference, we include here a brief discussion of the relation of the assumptions in

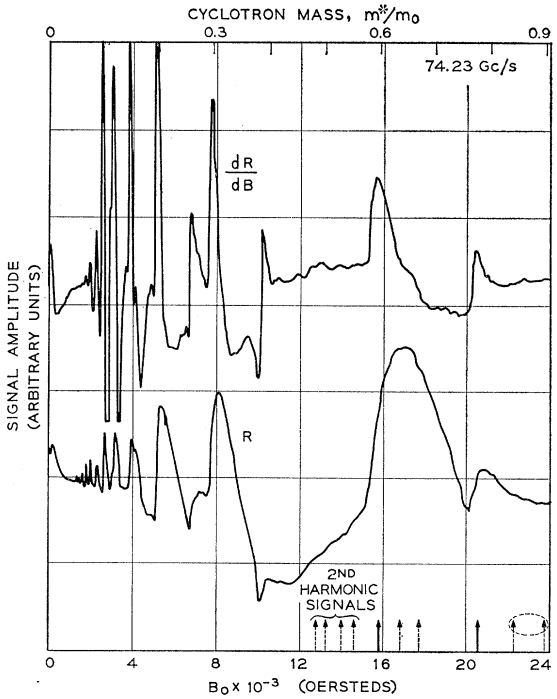

FIG. 2. Example of raw data obtained at 74.2 kMc/sec and 1.5°K. These data were obtained with the steady applied magnetic field B_0 at the crystallographic orientation represented by 58° in Fig. 4, as were those shown in Fig. 1. The lower curve shows the variation in the surface impedance R of cadmium on an arbitrary scale as a function of B_0 under these conditions directly on an arbitrary scale. The upper curve shows an experimentally observed derivative of this same quantity with respect to magnetic field, dR/dB, also on an arbitrary scale. The variation observed very near zero field has not been studied in detail, but is thought to be due to sample heating. The cyclotron mass corresponding to resonance at each value of B_0 is plotted at the top of the figure.

[13] M. C. Jones and E. Sondheimer, *The Fermi Surface*, edited by W. A. Harrison and M. B. Webb, (John Wiley & Sons, Inc., 1960); Proc. Roy. Soc. (London) **A278**, 256 (1964).

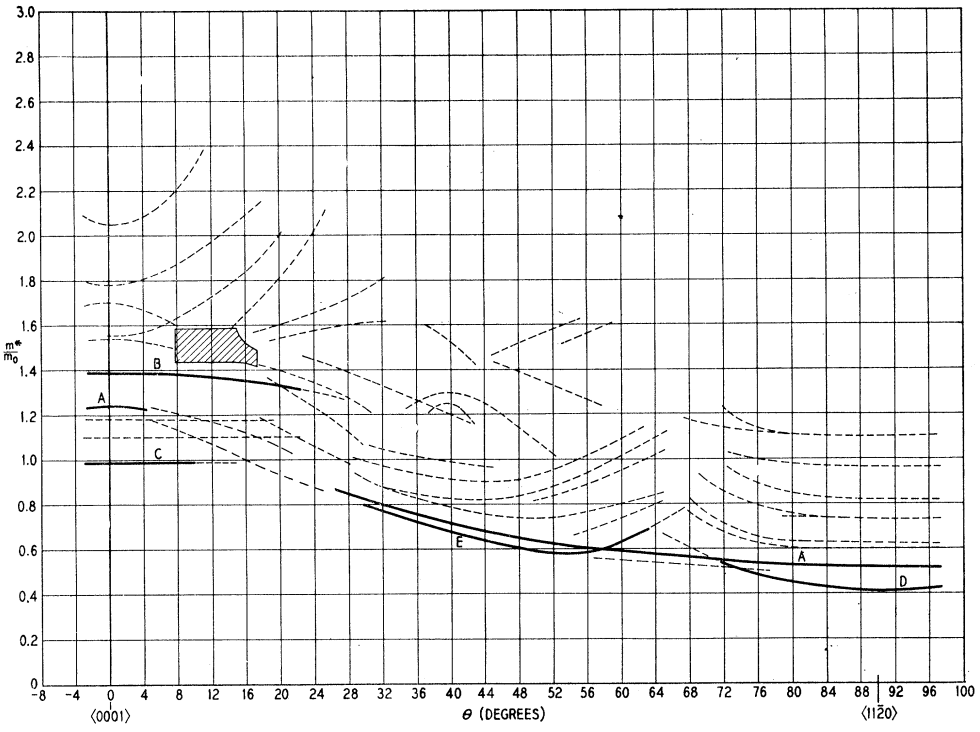

FIG. 3. Plot of the ratio of cyclotron effective masses to free-electron mass in cadmium versus the orientation of B_0 in the $\langle 10\bar{1}0\rangle$ plane. The orientations of B_0 shown are between the $\langle 0001\rangle$ and the $\langle 11\bar{2}0\rangle$ directions. This angular interval includes all nonequivalent orientations in the plane.

these two theories to our experiments. The critical variable which determines the extent and nature of the anomalous skin effect is ξ defined thus:

$$\xi = i\alpha/[1+i(\omega-\omega_c)\tau]^3, \tag{2}$$

where ω is the experimental frequency, ω_c is the cyclotron frequency, τ is the carrier relaxation time, $\alpha = 3l^2/2\delta^2$, l is the carrier mean free path and δ is the classical skin depth. In rationalized mks units

$$\alpha = 3l^2/[2(2/\omega\mu\sigma)] = (\tfrac{3}{4})l^2\omega\mu\sigma,$$
$$\omega_c = eB/m^*, \tag{3}$$

where σ is the dc conductivity. The Jones-Sondheimer theory assumes that α is very large, but because $\omega\tau$ is large, $\xi<1$ except near resonance. In order to estimate the values of ξ relevant to our experiments, note that the conductivity of cadmium at room temperature is 1.33×10^7 mho/m, and is not impurity sensitive. Since the resistivity ratio of our cadmium is about 3×10^4, it has a $\sigma\cong4\times10^{11}$ mho/m under our experimental conditions. Gibbons and Falicov[9] have found that the mean free path in similar material is about 1 mm. These values lead, at 74.2 Gc/sec, to $\alpha=1.7\times10^{11}$. If we assume a Fermi velocity of about 10^8 cm/sec, the 1 mm mean free path gives $\tau=10^{-9}$ sec, and thus $\omega\tau=500$ at this frequency. This gives $\xi\cong10^3$, except near resonance. This is very different from $\xi\cong10^{11}$, which this value of α gives when $\omega\tau$ is small, but is by no means less than one as required for the validity of the Jones-Sondheimer calculation, so the relevance of their derivation is not clear. Recently, R. G. Chambers (private communication and to be published) has suggested that the shape of the signal can be explained with a theory similar to that of Azbel'-Kaner which assumes that the total surface impedance is dominated by a nonresonant contribution.

Data of the type shown in Figs. 1 and 2 have been analyzed for the values of the effective masses in the manner mentioned above at each angle over the indicated intervals. The masses have then been plotted as a function of angle in the three planes for which this was done. The most doubtful of the signals which are recorded as indicating an effective mass have as a minimum basis that some indication of their presence occurs over a range of neighboring angles. These results are shown in Figs. 3, 4, and 5. The data shown in Figs. 1 and 2 correspond to an angle of approixmately 58° on Fig. 4. The masses which the experimental data make it possible to identify quite satisfactorily are plotted as heavy solid lines. Those for which the data are sufficiently unsatisfactory to leave some doubt about their specific validity are plotted as dashed lines. The uncertainties left by the experimental data with respect to the masses indicated by these dashed lines varies greatly. In some cases the only real uncertainty concerns the quantitative value of the effective mass. In others, the actual existence of the signal is in doubt. In general, however, it may be said with confidence that there are effective masses in cadmium with values in the ranges indicated by the dashed lines in Figs. 3, 4, and 5. In fact it is almost certain that there are more masses

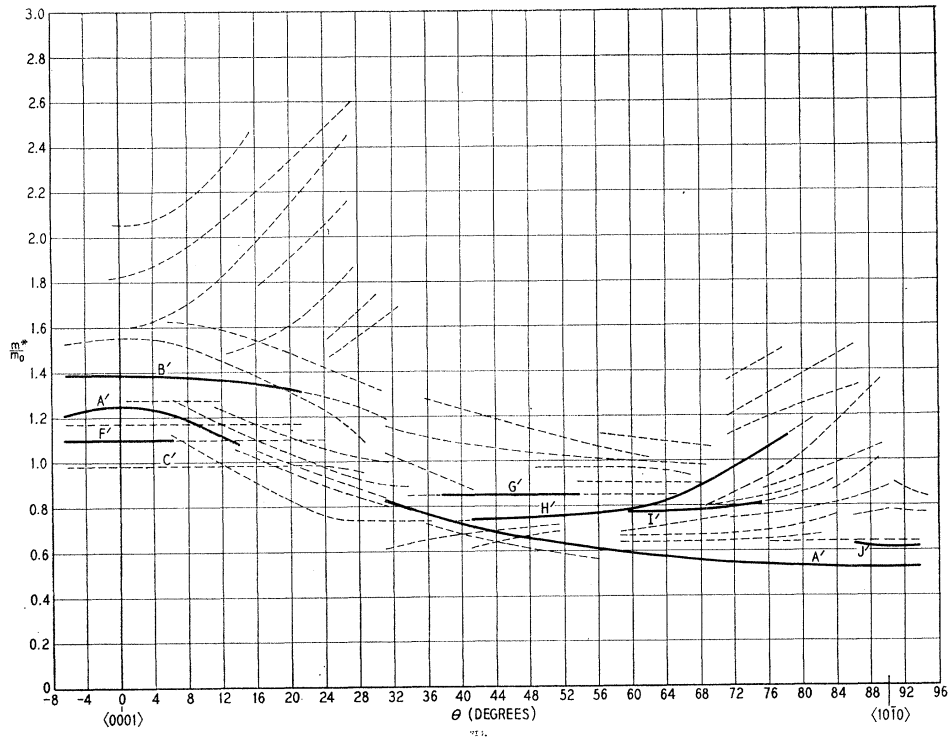

FIG. 4. Plot of the ratio of cyclotron effective masses to free-electron mass in cadmium versus the orientation of B_0 in the $\langle 11\bar{2}0\rangle$ plane. The orientations of B_0 shown are between the $\langle 0001\rangle$ and the $\langle 10\bar{1}0\rangle$ directions. This angular interval includes all nonequivalent directions in the plane.

present than these plots indicate. This will be discussed further in the next section. The various solid lines in Figs. 3, 4, and 5 are indexed by letters in order to simplify the discussion in Sec. IV, where tentative identification of the orbits relevant to each such line is made.

Some comment is called for on the relationship of the so-called peak-splitting phenomenon to the data presented in Figs. 3, 4, and 5. It has been found in experiments on tin, potassium, aluminum, and copper[14] under certain circumstances that when B_0 makes even a very small angle with the sample plane, the peaks in derivative curves of the type shown in Figs. 1 and 2 split, so that a carrier of one effective mass can give rise to what appears from the peaks associated with the fundamental resonance and its lower harmonics to be two masses. It is with a view to minimizing such effects that we have taken two experimental precautions: (1) the magnetic field and the sample plane have been aligned with considerable care to the precision described above and (2) the samples have been made very smooth and flat, also as described above.

There is evidence that in one specific case the peak-splitting phenomenon has distorted our data somewhat. We believe this explains the otherwise puzzling (large) signals which give the masses represented by dashed lines where gaps occur in the solid lines A and A′ in Figs. 3 and 4. This will be discussed in more detail later. On the other hand, we believe that as a result of the precautions mentioned above this phenomenon does not render any of the masses represented by solid lines in Figs. 3, 4, and 5 spurious. Some of the signals underlying these lines are broad, and we do not exclude the possibility that this is due to peak-splitting in some cases, although in others mass-spread may be involved. At worst, however, this only introduces uncertainties of a few percent in the numerical values of the masses; it does not suggest that the mass is spurious.

We now give several reasons for our conviction that the validity of the solid lines in Figs. 3, 4, and 5 is not substantially altered by the occurrence of peak splitting. First, we find that masses determined from the peaks are the same when 24 Gc/sec data are used as when 74 Gc/sec data are used. The different figures include results from separate experiments along principal axes which also contain checks. Second, the variation of the data with the orientation of B_0 represented by Figs. 3, 4, and 5 does not show pairs of peaks of comparable size varying in the same way with orientation if they are strong enough to justify representation by solid lines. Even in the case mentioned in the previous paragraph, the resolution and continuity in angle of the peaks do not justify two parallel solid lines. Third, the plots of harmonic number against $1/B_0$ for such resonances is linear in all cases to within experimental error. Noticeable deviations from this would be expected if the

[14] M. S. Khaikin, Zh. Eksperim. i Teor. Fiz. **42**, 27 (1962) [English transl.: Soviet Phys.—JETP **15**, 18 (1962)]; C. C. Grimes and A. F. Kip, Phys. Rev. **132**, 1991 (1963); C. C. Grimes, A. F. Kip, F. Spong, and R. A. Stradling, Phys. Rev. Letters **11**, 455 (1963); J. F. Koch, R. A. Stradling, and A. F. Kip, Phys. Rev. **133**, A240 (1964).

individual peaks were members of a split pair. In addition, we *have* observed the peak-splitting phenomenon in some earlier experiments performed before the precautions mentioned above were taken so carefully. These were experiments in which B_0 was near one of the principal crystallographic directions, and peak splitting was observed only when B_0 was near the $\langle 0001 \rangle$ direction, never when it was near $\langle 11\bar{2}0 \rangle$ or $\langle 10\bar{1}0 \rangle$. The phenomenon was observed fairly extensively at various angles of tip. The samples used in these early experiments were sufficiently convex so that the peak splitting did not in general disappear completely at any angle of tip, and the data are not presented here. The observed

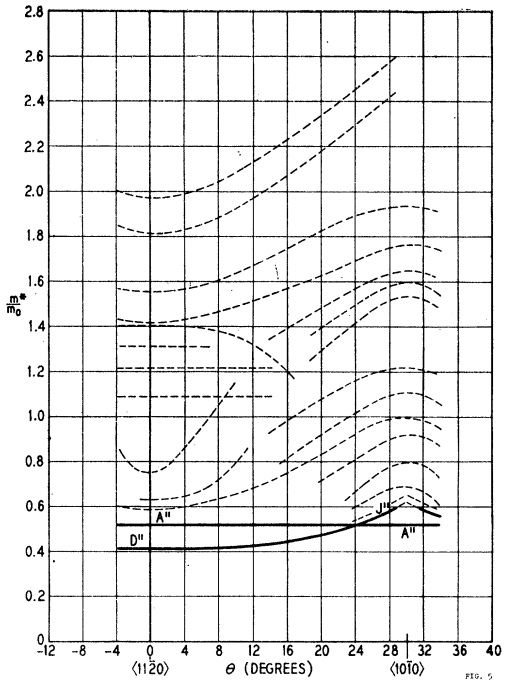

FIG. 5. Plot of the ratio of cyclotron effective masses to free-electron mass in cadmium versus the orientation of B_0 in the $\langle 0001 \rangle$ plane. The orientations of B_0 shown are between the $\langle 11\bar{2}0 \rangle$ and $\langle 10\bar{1}0 \rangle$ directions. This angular interval includes all nonequivalent directions in the plane.

peak splitting was in the resonance corresponding to the lines in Figs. 3 and 4 labeled A and A′ mentioned above, but for the $\langle 0001 \rangle$ direction where $m^*/m_0 = 1.25$. A naive interpretation of these peaks as resonances would have indicated masses above and below $m^*/m_0 = 1.25$. The later, more satisfactory data show that neither is a real mass.

It should be pointed out that some of the dashed lines associated with weak or poorly resolved signals do run parallel to one another in ways which could be a result of such an effect, although as will be seen in Sec. IV, we suspect that in many cases this is a result of partial magnetic breakdown and related effects. Further experiments would be required to explore and interpret these situations further.

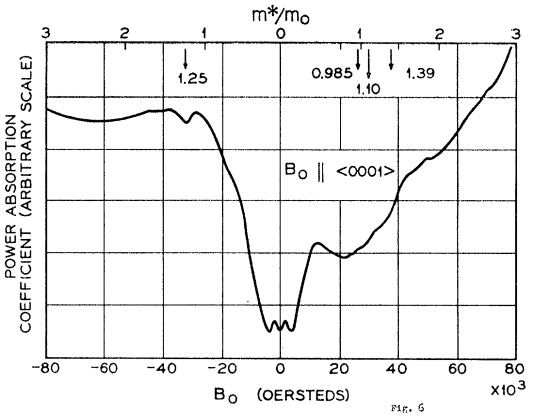

FIG. 6. Plot of variation in the real part of the surface impedance on an arbitrary scale as a function of steady applied magnetic field, B_0. These data were obtained at 1.5°K and 74.2 kMc/sec with B_0 normal to the sample surface and along the $\langle 0001 \rangle$ direction with circularly polarized radiation. The cyclotron mass corresponding to resonance at each value of B_0 is plotted at the top of the figure. Hole resonances occur at positive fields and electron resonances at negative fields.

As mentioned in the introduction, in addition to the results obtained in the Azbel'-Kaner geometry, data have also been taken with B_0 normal to the plane of the sample at both experimental frequencies. These experiments, however, have been done almost exclusively with the field along the three principal directions, $\langle 11\bar{2}0 \rangle$, $\langle 10\bar{1}0 \rangle$, and $\langle 0001 \rangle$. These results for the variation in the real part of the surface impedance are plotted directly on an arbitary scale in Figs. 6, 7, and 8. For simplicity, only the data obtained at 74.2 kMc/sec are presented. The results obtained in the experiments at 23.8 kMc/sec confirm these, but do not resolve the various features of the data as satisfactorily. In order to facilitate comparisons between the features of the

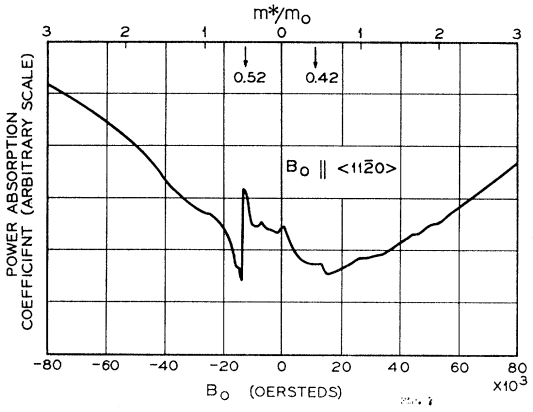

FIG. 7. Plot of variation in the real part of the surface impedance on an arbitrary scale as a function of steady applied magnetic field, B_0. These data were obtained at 1.5°K and 74.2 kMc/sec with B_0 normal to the sample surface and along the $\langle 11\bar{2}0 \rangle$ direction with circularly polarized radiation. The cyclotron mass corresponding to resonance at each value of B_0 is plotted at the top of the figure. Hole resonances occur at positive fields, electron resonances at negative fields.

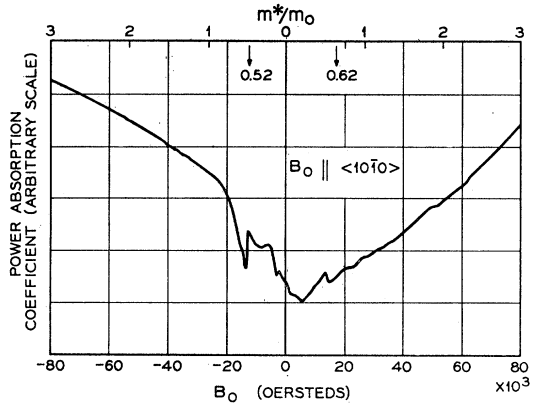

FIG. 8. Plot of variation in the real part of the surface impedance on an arbitrary scale as a function of steady applied magnetic field, B_0. These data were obtained at 1.5°K and 74.2 kMc/sec with B_0 normal to the sample surface along the $\langle 10\bar{1}0\rangle$ direction with circularly polarized radiation. The cyclotron mass corresponding to resonance at each value of B_0 is plotted at the top of the figure. Hole resonances occur at positive fields, electron resonances at negative fields.

data in Figs. 6, 7, and 8 with the masses shown in Figs. 3, 4, and 5, the abscissa in Figs. 6, 7, and 8 is shown in terms of m^*/m_0 as well as B_0. A discussion of these comparisons and of the significance of these data will be given in the next section.

IV. DISCUSSION

A. Relation of Data with B_0 Parallel to Sample Plane to Fermi Surface

The current model of the Fermi surface of cadmium is a modification of the free-electron Fermi surface given by Harrison.[3] The free-electron surface has been modified (1) to take account of spin-orbit coupling as discussed by Falicov and Cohen[4] and (2) to fit experimental data. A sketch of this model of the Fermi surface is shown in Fig. 9, reproduced from Ref. 9. The standard nomenclature for the various pieces of this surface is given in the caption of Fig. 9. In the free-electron model, the array of large sections at the corners of the zone are connected by waists, and thus form one large piece, called the "monster." It has been emphasized recently by Grassie[15] that when the waists are pinched off, as shown in Fig. 9, the various pieces (which we shall call "ears") assembled in groups of three around each vertical edge of the Brillouin zone form a large fluted sheet, of a different shape from the monster, which determines the path of many of the orbits in k space. Grassie has also proposed that while the model shown in Fig. 9 is correct when the magnitude of B_0 is small, at large B_0 magnetic breakdown occurs at the top and bottom of the fluted surface between it and another piece of the Fermi surface called a "cap," so that a significant deviation from Fig. 9 occurs. This deviation consists primarily of an enlargement of the vertical dimension of the unit cell in k space, but the important result is that the fluted surfaces do not connect to form a continuous chain in the c-axis direction when this happens. The shape of the fluted sheet under these circumstances is sketched in Fig. 10.

We will now discuss the relationship of this Fermi surface model to the results presented in Figs. 3, 4, and 5. The identification of specific orbits with specific solid lines in Figs. 3, 4, and 5 is in some cases tentative, but a plausible identification has been made in each case. No particular effort has been made to do this with respect to the results plotted as dashed lines in these figures in view of the unsatisfactory data on which they rest, although it is pointed out in various cases that the presence of partial breakdown is a plausible explanation for some of them.

Consider first Fig. 3, which shows the cyclotron masses as a function of the orientation of B_0 in the $(10\bar{1}0)$ plane, which includes the $\langle 0001\rangle$ and $\langle 11\bar{2}0\rangle$ directions. There is a curve, labeled A, which is solid except for a gap between 5° and 26°, and which goes from a mass of 1.25 m_0 when B_0 is along the $\langle 0001\rangle$ direction to 0.52 m_0 when it is along the $\langle 11\bar{2}0\rangle$ direction.

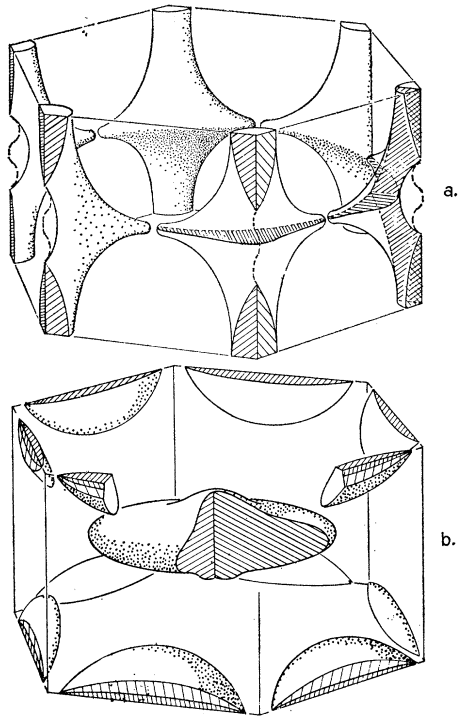

FIG. 9. Fermi surface for cadmium. (a) First band of holes are the large pieces at each of the six corners. These pieces arise from the "monster" of the simple free-electron model. The "caps" from the first band are shown cross-hatched. (b) Electrons from third and fourth bands. The "lens" or "pillow" is the piece centered in the cell. The other pieces are often called "butterflies" except for the cross-hatched pieces inside them which are called "cigars." This figure is after Fig. 10 in Ref. 9 except for the dashed lines which indicate that each piece associated with the second band holes touches the vertical edge of the zone at its center.

[15] A. D. C. Grassie, Phil. Mag. **9**, 847 (1964).

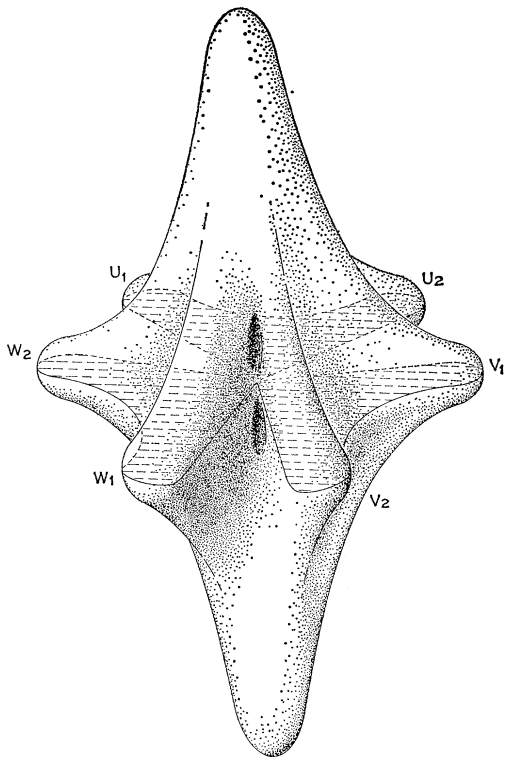

FIG. 10. Fluted surface made up of three of the pieces from the first band of holes clustered around one edge of the Brillouin zone. The part of this surface associated with one such piece is called an "ear" in the text. This figure is after Fig. 6 in Ref. 15, except that it touches the vertical axis at the equatorial plane.

At every orientation, the signal on which this curve is based is the largest one observed. In the gap between 5° and 26° there are two dashed lines, one on each side of the obvious extrapolation of the solid section of curve A, and these dashed lines are based on the largest signal at these angles. As mentioned earlier, we interpret these results to mean that peak splitting has distorted the resonance on which curve A is based in the region from 5° to 26°, and that there is one cylcotron mass for each orientation in this region whose value is given by the appropriate extrapolation of the solid curve into this region as discussed below. The curve outside the gap shows a variation in mass which fits that to be expected from an ellipsoidal section of Fermi surface quite well,[16] and this provides a method for carrying out the extrapolation into the gap. This has not been done in Fig. 3 in order to avoid added complexity in the figure, but the shape of the curve in this region may be found more precisely by examining the corresponding curve (A′) in Fig. 4, which is based on data in which this difficulty was much less serious in the sense that the two peaks were much closer together. The correspondence between curve A and that to be expected from an ellipsoid leads us to ascribe these masses to the "lens" or "pillow" which is at the center of the Brillouin zone shown in Fig. 9. It will be seen that this interpretation is consistent with the corresponding lines in Figs. 4 and 5. Our data are less sensitive than those of Gibbons and Falicov to the presence of such small deviations from ellipticity as the two bumps on the broad side of the pillow shown in Fig. 9. We find no evidence of them, presumably for this reason.

Before discussing the interpretation of the other solid lines one by one, it is appropriate to make a general comment. All these lines represent masses which are too large to identify plausibly with any of the small pieces of the Fermi surface in Fig. 9. Since we identify curve A with the "pillow," we are thus led to identify these masses with orbits on the large fluted surface shown in Fig. 10. It has, in fact, proved possible to make such identifications plausibly. We show in Fig. 11 two of the fluted surfaces properly related to one another, with representative orbits sketched on them, labeled to correspond to various lines in Figs. 3, 4, and 5. Note that when B_0 approaches 30° and 60° from $\langle 0001 \rangle$ in the $(10\bar{1}0)$ plane a considerable change in possible orbits would be expected if they are on the fluted surface. Such a change is clearly indicated in Fig. 3.

Consider now the line labeled B in Fig. 3. This line represents rather large but broad signals which are not very well resolved in the raw data. The effective mass given by this line is 1.38 m_0 when B_0 is along $\langle 0001 \rangle$, and it does not vary much as the orientation of B_0 changes, but the signal smears out and disappears when B_0 is about 20°–22° from $\langle 0001 \rangle$. There is also a line labeled C which indicates a mass of 0.98 m_0 for orientations of B_0 within about 10° of $\langle 0001 \rangle$ and which arises from relatively strong signals. Additional weaker signals are present and are indicated by dashed lines. We believe that the masses given by lines B and C and perhaps by some of the dashed lines have a related origin which we now take up.

We identify the mass shown by line B with orbits around the fluted surface in or near the equatorial plane, the same plane normal to the $\langle 0001 \rangle$ axis on which the pillow is centered. Such an orbit is shown in Fig. 11 and labeled B. Only an orbit of this type on this surface would be expected to have such a large mass. The presence of this orbit requires that the fluted surface contact the Brillouin zone boundary at the equatorial plane. This requires a small change in the earlier model of the Fermi surface which is similar to one suggested earlier by Stark in the case of zinc[17] on the basis of galvanomagnetic data. In this case, orbits mentioned in connection with de Haas–van Alphen[15,17] data and associated with arms of the fluted surface may still exist. Our data do not show them, but this may be because they are obscured by the higher harmonics of

[16] W. Shockley, Phys. Rev. **90**, 491 (1953).

[17] R. W. Stark, Phys. Rev. Letters **9**, 482 (1962); Phys. Rev. **135**, A1698 (1964).

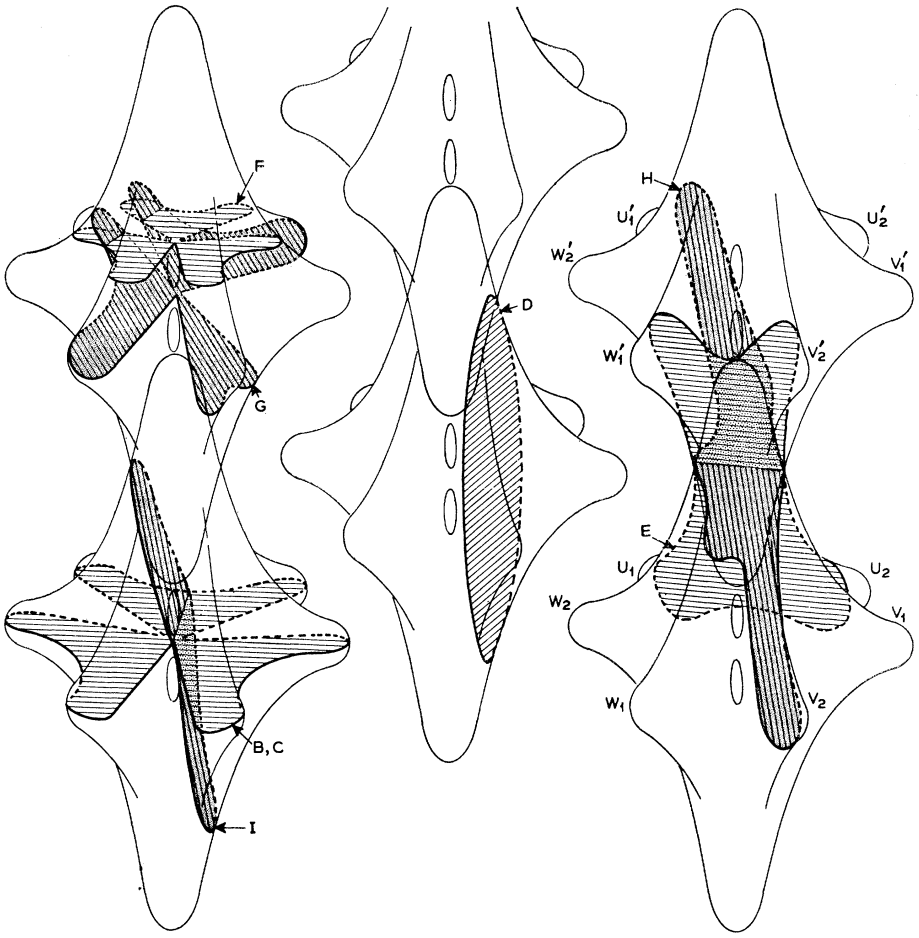

FIG. 11. Sketch of orbits associated with fluted surfaces. Orbits are labeled with letters as described in text. Note that several of the orbits involve two fluted surfaces of the type shown in Fig. 10.

other signals, since they should have a relatively low mass.[18]

Now consider the possibility that tunneling occurs in the equatorial plane where the fluted surface contacts the Brillouin zone boundary. If it occurs once during an orbit the orbit is smaller than the one described above, and an elementary argument suggests that a mass of roughly $(\frac{2}{3})1.38\ m_0 = 0.92\ m_0$ is to be expected. This is comparable with the observed value of $0.98\ m_0$ given by line C. We also note that two tunnelings per orbit lead to a mass of roughly $(\frac{4}{3})1.38\ m_0 = 1.84\ m_0$, and that in addition a mass of roughly $2.3\ m_0$ is possible. It seems plausible that such orbits can satisfactorily account for some of the masses represented by dashed lines for orientations of B_0 near the $\langle 0001 \rangle$ direction in Fig. 3.

When B_0 is along $\langle 11\bar{2}0 \rangle$, partial breakdown from the fluted surface to the caps at its top and bottom gives rise to a multiplicity of orbits such as the one labeled D in Fig. 11. Each such orbit is elongated along the c axis in the region near the center of the fluted surface where the three ears join. One of the vertical sides of the orbit is deep in a notch like that between points V_2 and W_1 on the fluted surface in Fig. 10, while the other is in the notch between U_2 and V_1. The lowest mass signal arises when the orbit is completed by magnetic breakdown at the first opportunity to the caps at the top and at the

[18] Since this report was written, we have learned privately of work done on cyclotron resonance in cadmium by T. G. Eck, M. P. Shaw, and D. Zych. They do not observe resonances corresponding to lines B and B′, but they do resolve two others at these orientations of B_0 with masses between these lines and lines A and A′. They have performed various experiments, some with linearly polarized radiation to show that one of these is a limiting point resonance, and occurs only when E_{rf} is parallel to B_0. They interpret this set of resonances to arise from the pillow electrons. These resonances are not resolved in our data, but indications of them do occur, as indicated by the horizontal dashed line between lines A′ and B′ in Fig. 4. We are now inclined to agree with their interpretation of the limiting point resonance, and to feel that this unresolved resonance is the correct explanation of our own observations with linearly polarized radiation rather than that given at the end of Sec. IVA. Our linear polarization experiments were performed at a time when the resolution of signals in our data was not adequate to distinguish between these signals and those underlying lines B and B′. This is not true of the latter data underlying Figs. 3, 4, and 5. We now also feel that the unresolved contribution of the limiting point resonance caused us to derive masses for lines B and B' which are low for orientations near $\langle 0001 \rangle$. These lines probably should cross this direction at m^* between 1.40 and 1.45. A preliminary report of the work of Shaw and Eck will be published in the *Proceedings of the Ninth International Conference on Low Temperature Physics* (Plenum Press, New York, to be published).

bottom. We identify orbits of this type with the masses plotted as line D in Fig. 3. It then seems possible that several of the signals with larger mass indicated by dashed lines in Fig. 4 arise from extensions of this orbit along the c axis to pass through two or more unit cells. These extended orbits stem from only a partial success of breakdown, and arise when the orbits are completed by breakdown at the second or later opportunity to the caps at the top and bottom of the fluted surface.

We now turn to the last of the solid lines plotted in Fig. 3, marked E. This we identify tentatively with an orbit of the sort marked E in Fig. 11 which passes between two of the fluted surfaces, i.e., a no-breakdown orbit. The bottom section of this orbit passes under two points on one ear of a fluted surface such as U_1 and U_2 in Fig. 10. It then passes, at an angle in the range 25–60° to the ⟨0001⟩ direction, to the unit cell just above where it passes *over* two points such as V_2 and W_1, which we call V_2' and W_1' to indicate that they are in a different unit cell. Note that V_2' and W_1' are from two different ears of the fluted surface and are thus not equivalent in orientation to U_1 and U_2. This orbit is only possible when B_0 is oriented in a range of angles between about 25° and 60° from the ⟨0001⟩ direction. It has a crossover where it passes between unit cells, and higher mass orbits can be constructed by assuming that breakdown occurs there. This may explain some of the dashed lines in Fig. 3 which run parallel to line E.

Consider now Fig. 4 which shows cyclotron masses as a function of the orientation of B_0 in the $(11\bar{2}0)$ plane, which includes ⟨0001⟩ and $\langle 10\bar{1}0\rangle$ directions. Here as in Fig. 3 there is a solid curve, labeled A′, which goes from a mass of 1.25 m_0 when B_0 is parallel to the ⟨0001⟩ direction to a mass of 0.52 m_0 when B_0 is normal to ⟨0001⟩, in this case along the $\langle 10\bar{1}0\rangle$ direction. Here again, the signals on which this curve is based are almost always the largest observed at any given angle, and their variation fits that to be expected from an ellipsoidal section of Fermi surface.[16] We therefore identify line A′ with the "pillow," as we did with the corresponding line in Fig. 3, which was labeled A. The numerical values of the masses read from the two curves are consistent with this interpretation, and with the symmetry and orientation of the "pillow." Also as in Fig. 3, there is evidence of peak splitting in Fig. 4, in this case in the range of angles from 14° to 31°. A gap in the solid line is shown in this region in Fig. 4, but the peaks, as the dashed lines in this region show, are much closer together than those in the data on which Fig. 3 is based, so that much less uncertainty is introduced into the masses in this case.

For orientations of B_0 near the ⟨0001⟩ direction in Fig. 4, there are also lines labeled B′ and C′ which correspond to lines B and C in Fig. 3 and which we interpret the same way. Line C′ is dashed in Fig. 4, as it is not as well resolved in these data as in those on which Fig. 3 is based. Here again the orbits are illustrated in Fig. 11.

There is in Fig. 4 a line F′ which is identical with a dashed line in Fig. 3 and which indicates the presence of a mass 1.10 m_0 independent of the orientation of B_0 in the neighborhood of the ⟨0001⟩ direction. The signals on which this line is based are not as well resolved as those underlying most of the solid lines in Figs. 3, 4, and 5. In spite of this uncertainty we tentatively identify it with orbits on the fluted surface of the sort labeled F in Fig. 11. It is parallel to the plane normal to the c axis, but intersects it above or below the equatorial plane. They are not really extremal orbits, but they are cut off rather sharply where the fluted surface loses contact with the edge of the Brillouin zone.

Next, line G′ in Fig. 4 indicates a mass of 0.85 m_0 for B_0 at angles of about 38° to about 54° from ⟨0001⟩. We suggest that the corresponding orbits are of the sort labeled G in Fig. 11. They are around the outside of the fluted surface in the plane normal to B_0 at each orientation which passes through the center of the fluted surface, i.e. the plane which intersects the c axis at the equatorial plane of this surface.

The masses shown by line H′ in Fig. 4 we interpret tentatively to arise from orbits like the one labeled H in Fig. 11. They go around two points, one on each of two fluted surfaces. For example, one point could be V_2 in Fig. 10. In this case, the other point would be U_1' on the fluted surface in the next unit cell above. Note that this is an orbit in which no breakdown occurs. None of the dashed lines in Fig. 4 are easy to interpret in terms of breakdown on this orbit.

Next line I′ in Fig. 4 shows masses which we identify with an orbit of the sort labeled I in Fig. 11. It goes from near the top of the fluted surface to correspondingly near its bottom. One side of the orbit passes between two such points as U_1 and U_2, both on the same ear of the fluted surface. The other side passes between two points such as V_2 and W_1, on different ears of the fluted surface. The orbit is on W_1 for the top of this side of the orbit, and on V_2 for the bottom, or vice versa. As the orientation of B_0 approaches the $\langle 10\bar{1}0\rangle$ direction in this plane, this orbit comes nearer the point of the fluted surface, and extended orbits tend to occur. Breakdown is required to achieve the original unextended orbit, which stays on one fluted surface, when B_0 is near the $\langle 10\bar{1}0\rangle$ direction. Perhaps for this reason, the signals are stronger when B_0 is not oriented very near this direction.

Lastly, consider orbits on the fluted surface in Fig. 10 obtained by rotating the normal to the D orbit shown in Fig. 11 about the c axis. It passes from deep in the notch between two such points as W_1 and V_2 on different ears behind two points like V_1 and V_2 to the notch between two such points as V_1 and U_2. We interpret the masses shown by line J′ in Fig. 4 to be due to such orbits on one fluted surface. It is possible that the plane of this orbit is such that a breakdown is required to keep the orbit on one fluted surface, but we are not sure.

Consider next Fig. 5, which has only two solid lines plotted. One, labeled A″, is consistent with line A in Fig. 3 and with line A′ in Fig. 4, and is therefore clearly to be identified with the "pillow". The line labeled J″-D″ is clearly consistent with the orbits in Fig. 11 which are associated with line D in Fig. 3, and with line J′, in Fig. 4.

We thus interpret all our principal signals obtained with the magnetic field parallel to the sample plane in terms of orbits on either the "pillow" or the fluted surface sections of the Fermi surface of cadmium. We observe no masses which we believe to be associated solely with the so-called "caps," or with the "butterflies," or "cigars" (see caption, Fig. 9). This is probably because the resonances associated with these sections are obscured by the higher harmonics of the resonances due to larger masses which we do observe.

Data were also obtained with linearly polarized microwave fields when B_0 was parallel to the sample plane and along each of the symmetry directions $\langle 0001\rangle$, $\langle 11\bar{2}0\rangle$, and $\langle 10\bar{1}0\rangle$. These data add very little information to that in the data on which Figs. 3, 4, and 5 are based. The data obtained with B_0 along $\langle 0001\rangle$, however, indicate that the orbits associated with lines B and B′ in Figs. 3 and 4, respectively, give stronger signals when the rf electric field is parallel to B_0 than when it is perpendicular. This suggests that most of the orbits involved do not go around the very ends of the points on the fluted surface, but are at slightly different values of k_z where there are components of velocity along $\langle 0001\rangle$. This suggests in turn that the rather broad shape of the resonances arises from mass spread among these orbits.[18]

B. Theory of Experiment with B_0 Perpendicular to Sample Plane

We now turn to the data obtained with B_0 perpendicular to the sample surface, shown in Figs. 6, 7, and 8. The principal effect indicated by these figures is an "opening up," or increase in the surface resistance, starting at field strengths B_0 which, as the vertical arrows in these figures show, correspond to classical cyclotron resonance conditions for masses substantially the same as those discussed above in connection with Figs. 3, 4, and 5. Moreover, the shape of the curve is not unlike that expected on the basis of an elementary classical theory based on the assumption of a local conductivity such as that given by Anderson.[19] We explain these results in terms of a relatively small effect associated with the charge carriers whose velocity is essentially parallel to the surface, as will be seen below.

These effects are somewhat surprising, however, in view of the fact that our samples are in the anomalous skin-effect regime, and of the work of Chambers[20] and Miller and Haering,[21] which is relevant to such experiments in this regime. By including the nonlocal relationship between field and current, these authors show that the cyclotron resonance in first approximation is broadened by the Doppler effect in the anomalous-skin-effect regime into a band. As a result, the large signal associated with cyclotron resonance is not observed at $\omega=\omega_c$, but at the edge of this band where $\omega_c=\omega+qv_F$. Here q is a characteristic wave vector of the electromagnetic wave and v_F is the Fermi velocity of the charge carriers; in the anomalous regime the wave vector q of the wave is very large. As the field B_0 is increased, q decreases until the above condition for the edge of the band is met, and a large change in surface impedance occurs. The field B_0 required to fulfill this condition in cadmium under the conditions of our experiments is, however, much larger than those available to us, and quite far removed from the field required to fulfill the condition $\omega=\omega_c$. We therefore propose an explanation for the existence of the signals in Figs. 6, 7, and 8 and then discuss them on the basis of this explanation.

It is important to note that the experimental curves in Figs. 6, 7, and 8 represent the variation in surface resistance, not with respect to a zero at the base line of the figures, but rather with respect to an arbitrary base line. Estimates of the absolute resistance lack the precision of the relative resistance data in Figs. 6, 7, and 8, but they indicate that the observed behavior reflects a change in surface resistance which is a small fraction of the total—perhaps 1 part in 10^3 or 10^4. As a consequence, the explanation of the behavior in Figs. 6, 7, and 8 is to be sought in understanding very small variations of the surface impedance rather than gross changes of the sort which primarily concerned the authors in Refs. 20 and 21.

Well below the Doppler-shifted edge of the resonance band where the present observations are made, the carriers primarily responsible for the surface impedance are those with the velocities nearly parallel to the surface. This has been shown by Pippard[22] in developing the ineffectiveness concept, which accounts for the anomalous skin effect phenomenologically. On physical grounds it is reasonable to expect that these carriers retain a resonance at $\omega=\omega_c$, since the presence of B_0 normal to the sample surface would not be expected to cause this group of carriers, whose velocity is normal to the electromagnetic wave, to deviate from classical behavior. On the other hand, as Pippard shows, the *number* of such carriers changes with τ and hence with $\omega_c\tau$ in just such a way as to cancel the change in the conductivity of each carrier with $\omega_c\tau$ in first approximation. This cancellation, which is most critical in the vicinity of the classical resonance where the changes in the conductivity of one carrier are most rapid, causes the surface impedance to be independent of B_0 in first

[19] P. W. Anderson, Phys. Rev. **100**, 749 (1955).
[20] R. G. Chambers, Phil. Mag. **1**, 459 (1956).
[21] P. B. Miller and R. R. Haering, Phys. Rev. **128**, 126 (1962).
[22] A. B. Pippard, Proc. Roy. Soc. **A191**, 385 (1947); **A191**, 399 (1947); Phil. Trans. Roy. Soc. (London) **250**, 325 (1957).

approximation. It remains possible, however, that in a higher approximation a small residual field dependence occurs, as we suggest, due to small deviations from this perfect cancellation, and this field dependence would be expected to be related to the classical resonance.

To make these arguments quantitative, we appeal to the analyses of the anomalous skin effect by Reuter and Sondheimer,[23] and by Dingle,[24] which were also used by Chambers.[20] In choosing the relevant mathematical formulation of the problem, care must be given to the choice of the boundary conditions since secondary effects are important. Separate closed formulas have been worked out by Dingle[24] for the surface impedance under conditions both of specular and of diffuse reflection of the carriers at the sample surface. As we have seen in Sec. III, the value of $\alpha=3l^2/2\delta^2$ in the present experiments is probably of order 10^{11}. The asymptotic form of the surface impedance for one group of isotropic charge carriers, under conditions where ξ in Eq. (2) is large, is given by these series expressions. For specular reflection, the surface resistance is given by

$$Z_1=8i\omega lc^{-2}w^{-1}\int_0^\infty \frac{dt}{t^2+i\alpha w^{-3}\kappa(t)},$$

$$\simeq(4\pi i\omega l/c^2w)\{0.7698(\pi i\alpha)^{-1/3}w+0.6534(\pi i\alpha)^{-2/3}w^2$$

$$+(\pi i\alpha)^{-1}w^3[0.1318\ln(\pi i\alpha/w^3)+0.0852]+\cdots\}, \quad (4)$$

where

$$w\equiv 1+i(\omega-\omega_c)\tau\equiv 1+i\omega'\tau, \quad (5)$$

$$\kappa(t)\equiv 2t^{-3}[(1+t^2)\tan^{-1}t-t]. \quad (6)$$

For diffuse reflection, the surface resistance is instead given by

$$Z_0=4\pi^2 i\omega lc^{-2}w^{-1}\Big/\int_0^\infty \ln[1+i\alpha w^{-3}t^{-2}\kappa(t)]dt,$$

$$\simeq(4\pi i\omega l/c^2w)\{0.866(\pi i\alpha)^{-1/3}w+(\pi i\alpha)^{-2/3}w^2$$

$$\times[0.1013\ln(\pi i\alpha/w^3)+0.3991]+\cdots\}. \quad (7)$$

The leading term in each series is practically the same, as is well known.[23] This confirms that the major effect is independent of the nature of the scattering at the surface. On the other hand, the effect we seek—a singularity or nonanalytic behavior in the variable $w=(1+i\omega'\tau)$ such as a $\ln w$ term—occurs with a coefficient of α^{-1} for specular reflection, while it occurs with a coefficient of $\alpha^{-2/3}$ for diffuse scattering; thus, for our purpose the two cases are rather different. In computing their respective curves, Chambers[20] assumed diffuse scattering while Miller and Haering[21] assumed specular scattering. Diffuse reflection seems the more appropriate assumption for those electrons with velocities parallel to the surface whose effects interest us most. This choice also conforms with the experimental work of Pippard,[22] whose results tend to favor the diffuse reflection assumption.

Let us therefore examine more closely the real part R_0 of Eq. (7) in the asymptotic regime, where

$$R_0=(4\pi\omega l/c^2(\pi\alpha)^{1/3})[0.433+0.1013(\pi\alpha)^{-1/3}$$

$$\times(\tfrac{1}{2}\sqrt{3}X-\tfrac{1}{2}X\omega'\tau-\tfrac{1}{2}Y-\tfrac{1}{2}\sqrt{3}Y\omega'\tau)$$

$$+0.3991(\pi\alpha)^{-1/3}(\tfrac{1}{2}\sqrt{3}-\tfrac{1}{2}\omega'\tau)]. \quad (8)$$

Here

$$X+iY\equiv\ln[\pi i\alpha/(1+i\omega'\tau)^3]. \quad (9)$$

The first term is independent of field, while the higher order terms contain the field-dependent effect. Roughly, these latter terms are reduced in magnitude near classical resonance by $\alpha^{1/3}\approx 10^3-10^4$, in reasonable agreement with our expectations. Equation (8) is most accurate in the general vicinity of classical resonance, which is the present range of interest.

Figure 12 displays the field-dependent component of R_0 as given by Eq. (8). Its similarity to the behavior associated with cyclotron resonance in this geometry for a single isotropic carrier under classical conditions is apparent.[19] This similarity supports our interpretation of the broad rise at high B_0 as due to quasiclassical behavior of electrons for one sign of B_0 and holes for the other. In the case of Figs. 7 and 8, Figs. 3, 4, and 5 show that two such carriers are dominant among the high-mass carriers which determine the behavior of the surface impedance at high B_0. The situation is more complicated in Fig. 6, but the existence of a broad rise for both directions of B_0 is confirmed by 23.8 Gc/sec data not shown in which all resonances are at lower B_0.

The data displayed in Figs. 6, 7, and 8 are clearly too complicated, however, to be understood simply in terms of the curve shown in Fig. 12. This not only reflects the fact that the two carriers mentioned above are present simultaneously, but also that other carriers are present and that the carriers are in general anisotropic. Among the other carriers involved are those from other pieces of the Fermi surface such as the butterflies, the cigars or the caps in Fig. 9, all of which are expected to have smaller masses than the two carriers mentioned above. It is reasonable that signals from these carriers were obscured in the data underlying Figs. 3, 4, and 5 by the harmonics of the higher mass carriers. Figs. 7 and 8 show a rise in surface impedance in the low-field region which we attribute to several small unresolved resonances associated with these carriers but which we are unable to analyze in any detail. This region in Figs. 7 and 8 extends up to the resonance fields of the higher mass carriers, and is ended by a very sharp drop on the electron resonance side at the resonance field associated with the pillow orbits. In Fig. 6, however, with B_0 along the hexagonal axis, the six butterfly

[23] G. E. H. Reuter and E. H. Sondheimer, Proc. Roy. Soc. (London) **A195**, 336 (1948).

[24] R. B. Dingle, Physica **19**, 311 (1953); Appl. Sci. Res. Sect. B, **3**, 69 (1952–1954); see also A. N. Gordon and E. H. Sondheimer Appl. Sci. Res. Sect. B. **3**, 297 (1952–1954).

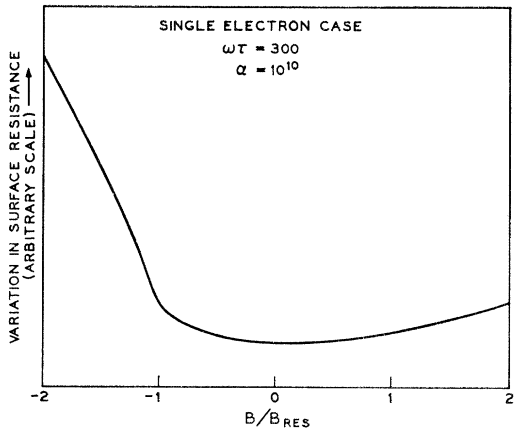

FIG. 12. Plot of variation of real part of Z_0 as calculated from Eq. (8) for the parameters shown and for a range of magnetic field which extends from fields above classical cyclotron resonance through zero to values where the direction of the field is such that no classical resonance occurs. Resonance is at $B/B_{\rm res}=-1$.

sections of the Fermi surface are equivalent, as are the six cigars and the six caps. This equivalence between various pieces of the Fermi surface might be expected to simplify our data in the low-field region, and there is evidence that it does. In the low-field region in Fig. 6 we see for both directions of B_0 a sharp change in slope at a field of 5.7 kG which corresponds to a mass of 0.22 m_0. By analogy with Fig. 12 and the classical case in the neighborhood of cyclotron resonance, we conclude that resonances occur at these two points and that these resonances determine the behavior in this low-field region. We suspect that one of these resonances is associated with electrons on the caps and the other with a hole orbit on the fluted surface outside the caps, since the shape of these sections of Fermi surface is such that a substantial number of the orbits on them would have zero velocity along B_0 in this case. In the absence of further information, however, this must be regarded as a tentative suggestion. We cannot be sure that these resonances are not both due to anisotropic orbits on the butterflies, for example.

The separation of the resonances of the low-mass carriers from those of the others present has facilitated their identification. It has not, however, made easier the next step in relating the over-all curve to one derived theoretically. We have found it more convenient in taking this step to compare theoretical curves with Figs. 7 and 8, as will be seen below.

In order to produce theoretical curves a step closer in complexity to that of the data in Figs. 6, 7, and 8, we have rederived the surface impedance for the case of *two* groups of isotropic-charge carriers whose contributions to the conductivity are additive. It would clearly be preferable to take account of the anisotropy of the carriers, but this is not a practical theoretical possibility. This approximation would be quite serious if the anisotropy were such for an important group of carriers that all their orbits had a net average velocity normal to the sample plane significantly different from zero, since the effect with which we are concerned is primarily due to orbits for which this velocity is approximately zero. Such a difficulty clearly does not arise in the case of the "pillow" orbits and the low-mass carrier orbits which are relevant to Figs. 7 and 8. For the D and J orbits, the situation is not so clear. However, while the average velocity of the D and J orbits which are extremal may not be zero, there are neighboring orbits for which it is. These are not violently different in effective mass, and while the effect observed with B_0 normal to the sample surface may be associated primarily with them, this should not cause our results to deviate wildly from reality.

If the subscripts 1 and 2 refer to the two carriers, then Eq. (7) becomes

$$Z_0=4\pi^2 i\omega l_1 c^{-2}\Big/\int_0^\infty \ln[1+i\alpha_1 t^{-2}K(t)]dt;$$

$$K(t)\equiv(n_1/w_1)\kappa(t/w_1)+(n_2/w_2)(m_1{}^*\tau_2/m_2{}^*\tau_1)\times\kappa(tl_2/l_1w_2), \quad (10)$$

where n_i is the fractional number of the ith carrier, $n_1+n_2=1$, and w_i is w of Eq. (5) for the ith carrier. In the limit of large α_1 (which is adequate for our purposes since we are interested in the impedance near both resonances) the analog of the series expansion shown in Eq. (7) reads, for the reciprocal of Z_0,

$$Z_0^{-1}=(c^2/4\pi i\omega l_1)\left\{(2/\sqrt{3})(i\pi\alpha_1)^{1/3}-(\tfrac{4}{3}\pi^2)\bar{w}\ln(i\pi\alpha_1/\bar{w}^3)-\pi^{-1}\int_0^\infty[tK'/K+1-4\pi^{-1}\bar{w}t^2/(t^3+\bar{w}^3)]dt\right\}, \quad (11)$$

where

$$\bar{w}=n_1w_1+n_2w_2; \quad K'=dK/dt.$$

Equation (11) is much more complicated than Eq. (8) in view of the greater number of free parameters. As with Eq. (8), it is most accurate in the general vicinity of classical cyclotron resonance. It is noteworthy that the leading term remains field independent as in (8), while the field-dependent terms are reduced in amplitude by the factor $\alpha^{1/3}\approx 10^3-10^4$ near classical resonance.

The plots of the real part of Z_0 from Eq. (11) still cannot be used, of course, to fit the data in Figs. 6, 7, and 8 directly. However, it is possible to reproduce many of the features of these curves by calculating Z_0 from Eq. (11) using parameters associated with various pairs of the carriers represented by the data. A substantial number of such calculations have been made with the aid of a computer, and their similarity to various features of Figs. 6, 7, and 8 strengthens our conviction that in principle the theory presented here explains the data. An example is shown in Fig. 13, which we compare below with Fig. 7.

Consider first the lower curve in Fig. 13. This curve

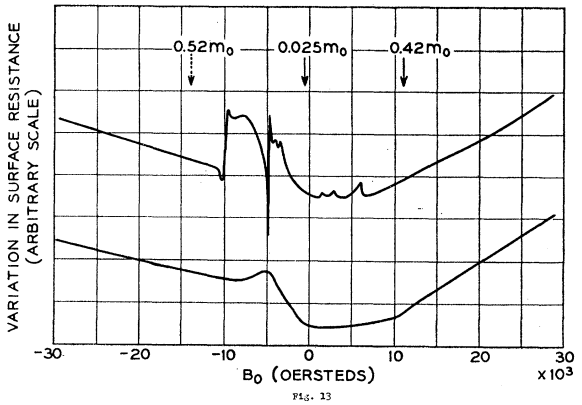

FIG. 13. Plots of variation in the real part of Z_0 calculated for two isotropic carriers from Eq. (11). The differences between the two curves are due simply to the fact that coarser intervals were used in calculating the integral in Eq. (11) for the upper curve. The two carriers were chosen as a hole of mass $0.42m_0$ and an electron of mass $0.025m_0$. Vertical solid arrows show the classical cyclotron resonance fields for these carriers. The dotted vertical arrow shows the position of this field for the pillow orbits relevant to Fig. 7. The parameters in Eqs. (10) and (11) were chosen so that $\alpha_1=1.8\times10^{10}$, $m_1=0.025m_0$, $m_2=0.42m_0$, $n_1=0.195$, $n_2\times(m_1^*\tau_2/m_2^*\tau_1)=0.363$, $l_2/l_1=1$, $\omega\tau_1=34$, $\omega\tau_2=255$, $\omega=4.5\times10^{11}$.

is calculated for a pair of carriers consisting of a majority carrier which is a hole of mass 0.42 m_0 as shown in Fig. 7 and a minority carrier which is an electron of mass 0.025 m_0 to represent crudely the low-mass carriers. It ignores the electrons of mass 0.52 m_0 indicated by an arrow in Fig. 7, and clearly present in the data underlying Figs. 3, 4, and 5. The crude assumption about the low-mass carriers and the failure to take account of the pillow electrons lead us to expect differences between the curves in Fig. 13 and Fig. 7, but in fact they do show remarkable qualitative similarities which seem to us to confirm the remarks made above. In particular, the broad rise at high fields apparent in Fig. 7 is also present in Fig. 13. On the hole (positive B_0) side, this is the main feature of both curves. This is characteristic of theoretical curves in which the hole is a majority; the relationship between majority and minority carriers, however, is complicated here by the fact that in the anomalous regime the number of *effective* carriers is affected rather more by the relaxation time assumed than by the total number of each type of carrier. In neither Fig. 7 nor in Fig. 13 is the hole resonance point marked by a particularly sharp feature of the curve. Just at zero field the curves differ, but above the electron resonance the theoretical curve rises to a small peak and then settles down to a plateau which we identify with the level region at low fields in Fig. 7. This plateau ends in the experimental data with a large and very sharp change which is much like a Lorentzian dispersion curve at the classical resonance field of the third carrier present. Since the theory ignores this third carrier, it is not surprising that this feature is absent from the lower curve in Fig. 13. It is, however, possible to suggest in terms of the theory how the third carrier produces this feature of the curve.

To take this next step, consider the upper curve in Fig. 13. This curve is derived from Eq. (11) with exactly the same parameters as the lower one. It is different only because the integration routine was carried out with coarser intervals. Here, considerable structure occurs in the region where the lower curve has a plateau, and this structure ends with a sharp drop. The differences between the two curves in Fig. 13 reflect the fact that the integral in Eq. (11) has very large terms of an oscillatory nature which cancel in certain ways, but which make it necessary to calculate the integral with great care. Even in calculating the lower curve there was some weak structure near the peak above the electron resonance which the curve does not show. It is of physical interest to note that the sharp drop which terminates this spurious structure in the upper curve in Fig. 13 always is associated with a dielectric anomaly in the relevant classical dielectric constant (a point at which the real part of the classical dielectric constant passes through one[12]), which gives rise to real features of similar data relevant to the classical regime. The sharp drop in the upper curve of Fig. 13 is very similar to the one in the data shown in Fig. 7 at the resonance field of the pillow electrons, but it is at lower B_0. It seems clear that the presence of the resonance of a third carrier in the neighborhood of a point which would be a dielectric anomaly if only the other two were present can alter the delicate balance among the terms in the intergral in Eq. (11). We suggest that this occurs in the situation underlying Fig. 7 in such a way as to move the location of the dielectric anomaly and make some of the structure in the upper curve of Fig. 13 real. This is then proposed as the basic explanation of the very sharp feature of the data in both Figs. 7 and 8 which occurs at the resonance field of the pillow electrons. This explanation is further confirmed by the fact that curves plotted from Eq. (11) for two electrons like those underlying Fig. 7 (and ignoring the holes) do not show this sharp feature at all. Thus it is suggested that most of the features of Fig. 7 can be understood in terms of the theory underlying Fig. 13.

ACKNOWLEDGMENTS

The authors wish to express their gratitude to P. H. Schmidt for growing the cadmium crystals and preparing flat, well-oriented samples; to D. Dorsi for zone refining the cadmium; to C. C. Grimes for an instructive conversation; to H. Dail for technical assistance; and to S. J. Buchsbaum, E. I. Blount, R. G. Chambers, T. G. Eck, E. A. Fawcett, C. C. Grimes, P. M. Platzman, P. L. Richards, and W. M. Walsh, Jr. for critical comments on the manuscript. Finally, C. J. Jernstedt has been most helpful in working out and executing Figs. 9, 10, and 11.